


# High spatial resolution mapping identifies habitat characteristics of the invasive vine *Antigonon leptopus* on St. Eustatius (Lesser Antilles)

Elizabeth A. Haber<sup>1</sup> | Maria J. Santos<sup>2,3</sup> | Pedro J. Leitão<sup>4,5</sup> | Marcel Schwieder<sup>5</sup> | Pieter Ketner<sup>6</sup> | Joris Ernst<sup>7</sup> | Max Rietkerk<sup>1</sup> | Martin J. Wassen<sup>1</sup> | Maarten B. Eppinga<sup>2,3</sup> 

<sup>1</sup>Copernicus Institute of Sustainable Development, Faculty of Geosciences, Utrecht University, Utrecht, The Netherlands

<sup>2</sup>Department of Geography, University of Zürich, Zürich, Switzerland

<sup>3</sup>University Research Priority Program in Global Change and Biodiversity, University of Zurich, Zürich, Switzerland

<sup>4</sup>Department Landscape Ecology and Environmental System Analysis, Institute of Geoecology, Technische Universität Braunschweig, Braunschweig, Germany

<sup>5</sup>Geography Department, Humboldt-Universität zu Berlin, Berlin, Germany

<sup>6</sup>Emeritus, Tropical Nature Conservation and Vertebrate Ecology Group, Department of Environmental Sciences, Wageningen University, The Netherlands

<sup>7</sup>WoestLand, Lichtenvoorde, The Netherlands

## Correspondence

Maarten B. Eppinga, Department of Geography, University of Zürich, Zürich, Switzerland.  
Email: maarten.eppinga@geo.uzh.ch

## Funding information

Nederlandse Organisatie voor Wetenschappelijk Onderzoek, Grant/Award Number: 858.14.052; Van Eeden Foundation, Grant/Award Number: 201509

**Associate Editor:** Jennifer Powers  
**Handling Editor:** Laura Schneider

## Abstract

On the Caribbean island of St. Eustatius, Coralita (*Antigonon leptopus*) is an aggressive invasive vine posing major biodiversity conservation concerns. The generation of distribution maps can address these conservation concerns by helping to elucidate the drivers of invasion. We test the use of support vector machines to map the distribution of Coralita on St. Eustatius at high spatial resolution and use this map to identify potential landscape and geomorphological factors associated with Coralita presence. This latter step was performed by comparing the actual distribution of Coralita patches to a random distribution of patches. To train the support vector machine algorithm, we used three vegetation indices and seven texture metrics derived from a 2014 WorldView-2 image. The resulting map shows that Coralita covered 3.18% of the island in 2014, corresponding to an area of 64 ha. The mapped distribution was highly accurate, with 93.2% overall accuracy (Coralita class producer's accuracy: 76.4%, user's accuracy: 86.2%). Using this classification map, we found that Coralita is not randomly distributed across the landscape, occurring significantly closer to roads and drainage channels, in areas with higher accumulated moisture, and on flatter slopes. Coralita was found more often than expected in grasslands, disturbed forest, and urban areas but was relatively rare in natural forest. These results highlight the ability of high spatial resolution data from sensors such as WorldView-2 to produce accurate invasive species, providing valuable information for predicting current and future spread risks and for early detection and removal plans.

Abstract in Dutch is available with online material.

## KEYWORDS

Caribbean, invasive species, landscape ecology, plant ecology, remote sensing, Support Vector Machine

This is an open access article under the terms of the Creative Commons Attribution-NonCommercial License, which permits use, distribution and reproduction in any medium, provided the original work is properly cited and is not used for commercial purposes.

© 2021 The Authors. *Biotropica* published by Wiley Periodicals LLC on behalf of Association for Tropical Biology and Conservation.

## 1 | INTRODUCTION

Invasive alien species (IAS) are an important driver of worldwide biodiversity loss, as successful invasions may lead to biotic homogenization at the expense of endemic species (Bellard et al. 2016; McKinney & Lockwood, 1999; Olden et al. 2004, Santos et al. 2011). The most profound impacts of IAS on biodiversity would therefore be expected in areas with high levels of endemism (Berglund et al. 2009; Sakai et al. 2001). Island archipelagos may exhibit such high levels of endemism, driven by unique evolutionary histories (Brown & Sax, 2004; Myers et al. 2000). These characteristics contribute to many islands being part of global biodiversity hotspots (Myers et al. 2000; Sloan et al. 2014), but also highlight their susceptibility to the impacts of IAS (Sakai et al. 2001; D'Antonio & Dudley, 2011; but see Vilà et al. 2011). The problem is particularly pronounced for (sub) tropical islands, where in some cases half of the plant species are now of exotic origin (Sax et al. 2002), and globally they are the recipients of disproportionate numbers of IAS (Turbelin et al. 2017).

Within (sub)tropical island systems, knowledge of the distribution of IAS at high spatial resolution is critical for understanding the local drivers of invasion and identification of areas at risk (Andrew & Ustin, 2009; Gottschalk et al. 2011). However, the need to collect data at high spatial resolution, while covering IAS distributions at the landscape scale, often limits the feasibility of traditional field sampling (Dronova et al. 2017). High spatial resolution remote sensing imagery provides a powerful, systematic, and repeatable method to identify and monitor the distribution of plant species at the landscape scale (He et al. 2011; Santos et al. 2016). Although imaging spectroscopy provides the most opportunities to distinguish invasive plants from native species (Santos & Ustin, 2018), its utilization to map IAS is still mostly restricted to handheld or airborne platforms (Asner et al. 2008; Asner, Knapp, et al., 2008 but see Somers & Asner 2012, 2013). In cases where the IAS is clearly detectable, however, it may also be detected with satellite sensors providing multispectral imagery (Santos & Ustin, 2018). For such IAS, this is a particularly promising option, as these sensors can cover large geographic extents and with high spatial resolution, at relatively low user costs (Huang & Asner, 2009; Robinson et al. 2016). Whether these advantages of multispectral imagery can be utilized depends on the ability to detect invasive species with the limited number of spectral bands (Dronova et al. 2017). In addition, the challenges involved in vegetation classification from multispectral imagery can be reduced by modern classification methods (Sluiter & Pebesma, 2010; Tarantino et al. 2019). Specifically, Support Vector Machines (SVMs) provide a robust image classification algorithm and have been successfully applied to infer IAS distributions. Although the ability of SVMs to detect IAS has been tested with high spatial resolution multispectral data (Cho et al. 2015; Pouteau et al. 2012; Xun & Wang, 2015) understanding the full potential of applying SVMs to mine these data requires further exploration (Royimani et al. 2019).

*Antigonon leptopus* (Hook. & Arn.), commonly known as Coralita, is a widespread invader of (sub)tropical regions around the world. This herbaceous perennial vine is originally from Mexico, and its

spread has been driven by its appeal as a cultivated garden plant (Burke & DiTommaso, 2011). The infestation of Coralita on the northern Caribbean island of St. Eustatius is arguably the most extreme example of this plant's invasive capability, with previous estimates (based on ground surveys) indicating that the plant appears on 15–33% of the island's area, although its cover does not reach 100% at all locations indicated in these studies (Berkowitz, 2014; Ernst & Ketner, 2007). Thus, understanding Coralita's geographic extent and the potential factors influencing its distribution on St. Eustatius are of high importance. Moreover, analyzing the associations between IAS presence and landscape and environmental characteristics is a crucial step toward identifying areas at risk of further invasion (Bartuszevige & Gorchoy, 2006).

In this study, we map the distribution of Coralita on St. Eustatius at high spatial resolution (i.e. 2 m by 2 m) and evaluate the potential associations of local environmental conditions with Coralita presence over the complete distribution of this population. We focus on five landscape and environmental characteristics that we hypothesize are associated with Coralita presence. Specifically, our goals for this study were to: (1) evaluate the potential of SVMs to accurately detect Coralita at high spatial resolution with WorldView-2 imagery and (2) identify fine-scale spatial associations between Coralita and several landscape and geomorphological variables which we hypothesize are linked to spread and persistence of Coralita. These analyses may serve to identify the fine-scale environmental conditions of habitats occupied by Coralita in non-native locations, and to assess the potential of the proposed approach for large-scale monitoring of this species.

## 2 | METHODS

### 2.1 | Study area

St. Eustatius (17°28' N, 62°58' W) is a small island (area ~21 km<sup>2</sup>) that is part of the Cenozoic lesser Antilles volcanic arc (Figure S1). The climate is tropical, with a mean annual temperature of 25.7°C and mean annual precipitation of 1073 mm (Rojer, 1997). Precipitation is likely higher on the slopes of the southern Quill volcano, which has a maximum height of 601 m (Rojer, 1997). The lower outer slopes of the Quill are covered by dry evergreen forests, (semi-) evergreen, and deciduous seasonal forests, whereas (secondary) rain forest can be found on the highest elevations (van Andel et al. 2016; de Freitas et al. 2014; Stoffers, 1956). Most of the island's bedrock is of volcanic origin, with clay loam soils in shallow areas and stonier and sandier loam soils on steeper slopes of both the northern and southern volcanic complexes (De Freitas et al. 2014; Veenenbos, 1955).

### 2.2 | Mapping Coralita distribution

The construction of a Coralita distribution map for St. Eustatius consisted of four steps (Figure 1; extended in Figure S5).

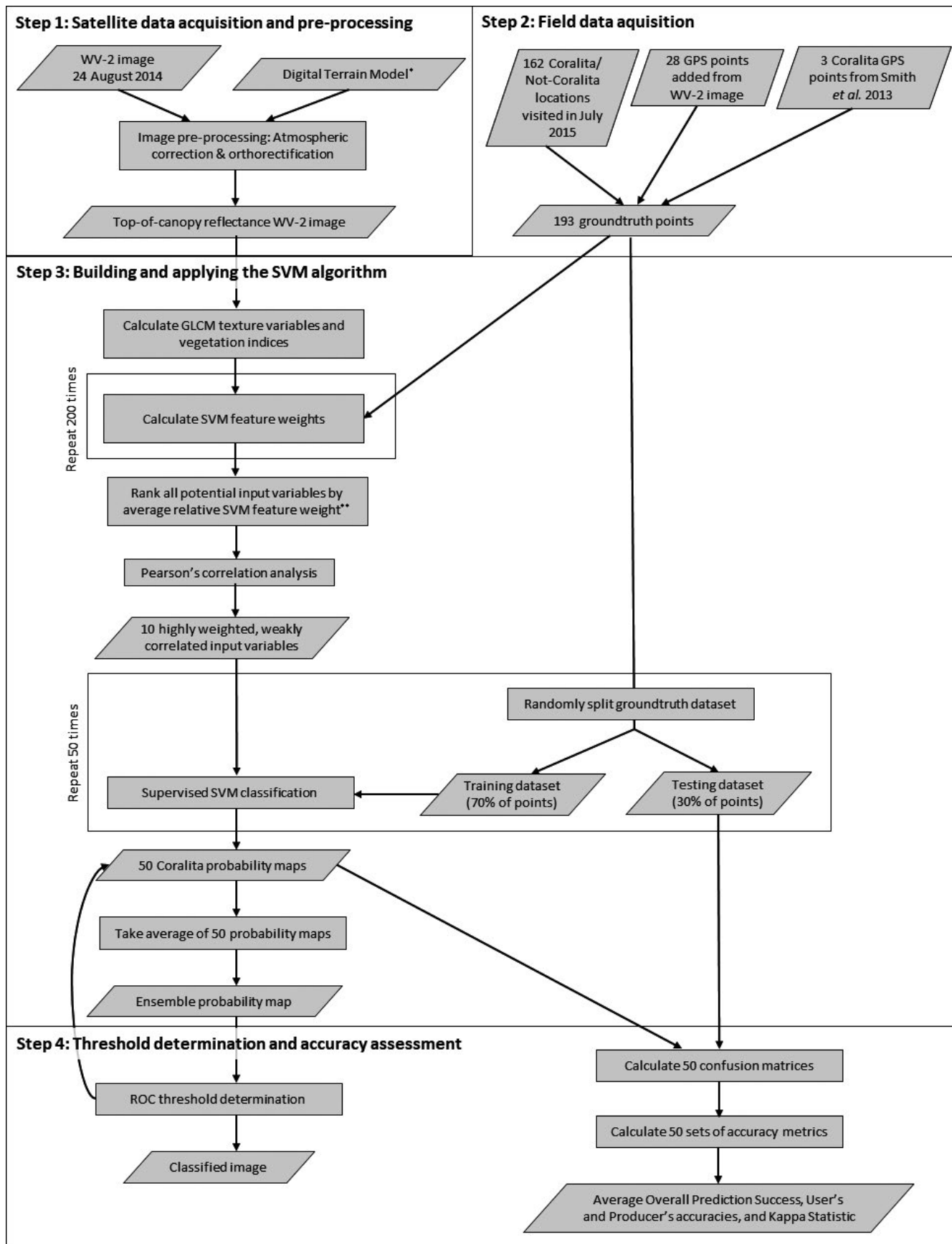


**FIGURE 1** Flowchart showing how a Coralita distribution map for St. Eustatius was developed, using a Support Vector Machine learning algorithm. The procedure consisted of Steps 1–4 described in the main text. A more detailed flowchart is provided in the Supplementary Information (Figure S5). Acronyms used in figure: WV-2: WorldView-2; GLCM: Gray-level co-occurrence matrix; ROC: Receiver operating characteristic. Asterisks indicate references: \*Mücher et al. (2014); \*\*Ustün et al. (2007)

### 2.2.1 | Step 1: Satellite data acquisition and pre-processing

The WorldView-2 satellite acquires high spatial resolution ( $2 \times 2$  m) images over 8 spectral bands, with six bands in the visible light spectrum and two bands in the near-infrared spectrum (DigitalGlobe Inc.). In the visible spectrum, four bands span the colors *Blue* (450–510 nm), *Green* (510–580 nm), *Yellow* (585–625 nm), and *Red* (630–690 nm), while two extra bands cover the visible light spectrum edges. First, the *Coastal* band (400–450 nm) distinguishes particular shades of blue and violet. Second, the *Red-edge* band (705–745 nm) covers the range of wavelengths in which vegetation's interaction with light changes rapidly from absorption to reflection. The two near-infrared bands are referred to as  $NIR_1$  (770–895 nm) and  $NIR_2$  (860–1040 nm). We used a cloud-free WorldView-2 image that was taken on 24 August 2014, which was orthorectified and atmospherically corrected (GIM, Leuven, Belgium, Supplementary Information).

### 2.2.2 | Step 2: Field data acquisition

We visited 162 sampling points on St. Eustatius in July 2015. Although there was a time difference of 11 months between the image and reference data collection, we assumed that Coralita patches that were present in 2014 persisted in 2015. We also assumed that Coralita-covered locations sampled in 2015 (typically near the Coralita patch centers) were already covered by Coralita in 2014. These assumptions are based on observations suggesting that the majority of Coralita growth is clonal via sprouting from tuberous storage structures buried in the soil (Ernst & Ketner, 2007). These characteristics create persistent Coralita patches, but they also constrain the rate of outward spread to a few meters per year (Ernst & Ketner, 2007). Moreover, no extreme events such as hurricanes occurred on the island during this period (Eppinga & Pucko, 2018). Sampling points were selected with a mixed procedure, with direct selection of target (i.e., Coralita) points to ensure sufficient representation and random selection of non-target points (i.e., other land cover types and landscape features). We visited  $n = 32$  points where Coralita was the dominant species, that is, occupying  $\geq 50\%$  of the surface/canopy area. These points were found using information from previous studies (Ernst & Ketner, 2007; Smith et al. 2013), and opportunistically while sampling other types of surface cover (see below). At the remaining  $n = 130$  sampling points, Coralita was not present. These points were sampled in a stratified random manner according to slope, to ensure that a variety of habitats and vegetation types was captured. Additionally, 28 not-Coralita sampling points of inaccessible features, such as building roofs, were visually inspected using the WorldView-2 image, and their coordinates were added to the reference data. We also included three Coralita points using GPS locations from three large Coralita patches recorded in a previous study (Smith et al. 2013). Thus, a total of 193 reference data points were used.

At each sampling point, geographic coordinates (datum: WGS1984) were recorded with a Trimble Geo7x handheld GNSS receiver (Trimble Inc.) at the corners and center of a  $4 \times 4$  m plot. This plot size ensured that at least one pixel of the WorldView-2 image was completely captured. One-minute measurements at each plot corner and center yielded 60 independent coordinate readings, which were later differentially corrected using data from the nearest Continuously Operating Reference Station (St. Maarten, 60 km from St. Eustatius) and the Trimble GPS Pathfinder Office software. This procedure yielded horizontal accuracies ranging from 0.1 to 12.1 m, with a median accuracy of 0.3 m.

### 2.2.3 | Step 3: Building and applying the SVM algorithm

In this step, the reference data were used to identify 35 Coralita and 158 not-Coralita pixels on the WorldView-2 image. As the image provides for each pixel the reflectance values for the eight spectral bands, a number of variables was derived to test their ability to effectively distinguish Coralita from not-Coralita pixels. In addition to the eight spectral bands, multiple spectral band values were combined into spectral indices. We considered 20 indices that were shown to be successful in classifying vegetation with WorldView-2 data (Nouri et al. 2014; Oumar & Mutanga, 2013, Table S1). Additional variables were also created by combining scores of neighboring pixels, thereby describing spatial patterning and heterogeneity in reflectance values (Haralick et al. 1973). Specifically, variable scores were converted to a gray scale, and the distribution of co-occurring pixel values was computed, creating a grayscale level co-occurrence matrix (GLCM). From the GLCM, a number of texture variables can be calculated (Haralick et al. 1973, Supplementary Information). Texture variables have also been shown to improve vegetation classifications (Khatami et al. 2016). In total, 92 candidate variables were considered: 8 spectral bands, 20 vegetation-based spectral indices and 64 texture variables. This pool of candidate variables was reduced to a set of 10 variables based on two criteria (Supplementary Information): (1) potential contribution to distinguishing Coralita pixels; (2) sufficient independence from other variables.

The selected 10 variables included three vegetation indices (Table 1): *Total Red-edge Slope* (TRES), NDVI of *Red-edge* and *Coastal* bands, and the ratio between the second near-infrared and red bands ( $NIR_2;Red$ ). Both TRES and  $NIR_2;Red$  describe differences in absorption of red and near-infrared wavelengths, which typically depend on chlorophyll content and other leaf properties (Horler et al. 1983; Walter-Shea & Norman, 1991). In contrast, the *Red-edge* and *Coastal* NDVI typically correlates with non-homogeneous (urban) features that stand out from the background landscape (Wolf, 2010). The remaining selected variables were seven texture variables (Table 1). Six of these texture variables described spatial patterning in red and near-infrared wavelength reflectance between neighboring cells. The remaining texture variable described spatial patterning in reflectance of the *Blue* band (Table 1). For each input variable, we compared the

TABLE 1 Input variables included in Coralita SVM model

Variable (SVM feature weight rank)	Definition	Test statistic Coralita – Not Coralita comparison (p-value)
Total red-edge slope (1)	The first derivative of reflectance between red and near infra-red wavelengths	$D_{35,158} = 0.800 (p < 0.001)$
GLCM mean <sub>Red-edge</sub> (2)	The mean value of the gray-tone spatial dependence matrix of the red-edge band	$D_{35,158} = 0.616 (p < 0.001)$
GLCM homogeneity <sub>Red</sub> (3)	The inverse square of the gray-tone spatial dependence matrix of the red band	$D_{35,158} = 0.331 (p = 0.003)$
NDVI <sub>Red-edge and Coastal</sub> (4)	A spectral index comprised of the normalized difference between the red-edge and coastal bands	$D_{35,158} = 0.500 (p < 0.001)$
GLCM entropy <sub>NIR1</sub> (5)	The negative logarithm of the probability mass function of the gray-tone spatial dependence matrix of the first near-infrared band	$D_{35,158} = 0.256 (p = 0.039)$
NIR <sub>2</sub> :Red (6)	The ratio of reflectance at near infra-red and red wavelengths	$D_{35,158} = 0.430 (p < 0.001)$
GLCM second moment <sub>Blue</sub> (7)	The sum of squares of the gray-tone spatial dependence matrix of the blue band	$D_{35,158} = 0.322 (p = 0.004)$
GLCM dissimilarity <sub>NIR1</sub> (8)	The probability mass function of the gray-tone spatial dependence matrix of the first near-infrared band, where each pixel pair is weighed according to the linear distance between pixels,	$D_{35,158} = 0.331 (p = 0.003)$
GLCM correlation <sub>Red</sub> (9)	The measure of linear dependence between pixels of the gray-tone spatial dependence matrix of the red band	$D_{35,158} = 0.278 (p = 0.019)$
GLCM correlation <sub>NIR1</sub> (10)	The measure of linear dependence between pixels of the gray-tone spatial dependence matrix of the first near infra-red band	$D_{35,158} = 0.230 (p = 0.083)$

Note: Input variables included in the SVM classification model ranked according to SVM relative feature weight. The first column lists the input variable names and the SVM feature weight ranking (for further information, see Methods section “Mapping the occurrence patterns of Coralita” and Supplementary Table S1). The second column defines the variables in terms of the WorldView-2 bands used to calculate them. The third column shows the results of two-sample Kolmogorov–Smirnov tests comparing the distributions of Coralita ( $n = 35$ ) and not-Coralita ( $n = 158$ ) points on each variable (as also shown in Figure 2).

Abbreviations: GLCM, gray-level co-occurrence matrix; NIR, near-infrared.

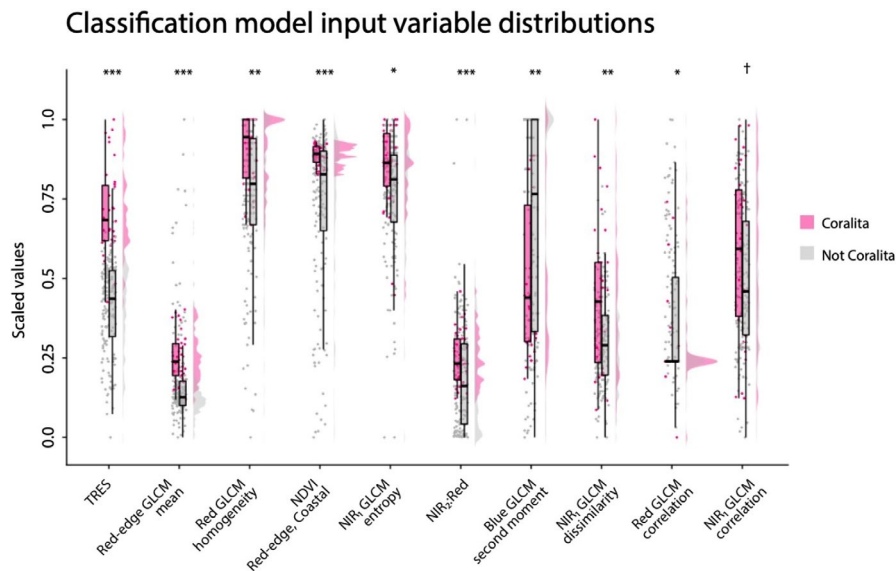


FIGURE 2 Plot displaying the distributions of values for the 10 input variables used to build and apply the Support Vector Machines model, separated by classification category. Data for each input variable are displayed by paired boxplots overlain with raw data points and probability distributions of the two classification categories. Variables TRES, Red-edge GLCM mean, NDVI Red-edge, Coastal, and NIR<sub>2</sub>:Red show the largest separation for the classification categories according to two-sampled Kolmogorov–Smirnov tests ( $p < 0.001$ ). Abbreviations used on x-axis: GLCM, Gray-Level Co-occurrence Matrix; NDVI, Normalized Difference Vegetation Index; NIR, near-infrared; TRES, Total Red-edge Slope. Colors refer to the corresponding WV-2 bands used to calculate the indices. Symbols indicate significant differences: \*\*\* $p < 0.001$ , \*\* $p < 0.01$ , \* $p < 0.05$ , † $p < 0.1$



distribution of values of Coralita and not-Coralita points using two-sample Kolmogorov–Smirnov tests.

Using the 10 input variables and the reference data (Figure 1), we employed a binary SVM classification distinguishing two classes: 'Coralita' and 'not-Coralita'. An SVM is a supervised non-parametric machine learning algorithm to classify image data into categories, such as vegetation types or species (Mountrakis et al. 2011). Support Vector Machines have been shown to successfully handle small training data sets, even with many input variables, and often outperform other classification or regression approaches (Khatami et al. 2016; Mantero et al., 2004; Schwieder et al. 2014). Through machine learning, support vectors are generated as combinations of input variables, with the aim of separating data points of different classes by a support vector hyperplane (Cortes & Vapnik, 1995). Importantly, support vectors consisting of linear combinations of input variables may not be effective in separating classes and creating a reliable classification (Sha & Bai, 2013). Instead, SVMs allow for considering a wide range of non-linear combinations of input variables by transforming them via a kernel operation (Rumpf et al. 2010).

The support vectors that best separated the two classes were found by tuning them to a subset of reference points used as training data. Specifically, we randomly split the 193 reference points into a training set (70%) and a testing set (30%). To enable non-linear combinations of input variables, we used a Gaussian radial basis function kernel. Within the SVM framework, tuning consists of optimizing two parameters. First, the *cost* parameter determines how strongly a model fit is penalized for incorrectly classifying training data points. Second, the *gamma* parameter controls the width of the kernel, and thereby the way in which data points are separated from each other (e.g. Mountrakis et al. 2011). In this study, optimal values for *cost* and *gamma* were searched for within a parameter search space bounded by  $e^{-5}$  -  $e^{15}$  and  $e^{-15}$  -  $e^3$  (using multiplicative step sizes of  $e^1$ ), respectively. The performance of the SVM is defined as its ability to correctly assign the training data to the Coralita and not-Coralita classes. As direct estimates of performance tend to overfit, a ten-fold cross-validation was performed (see Supplementary Information). The resulting optimized (i.e., best performing) set of support vectors was used in the final SVM model to predict the probabilities of Coralita presence over the entire image. The outcome of applying the SVM model is a map indicating the probability for each pixel of belonging to the Coralita class. The SVM model was tuned, built, and implemented in R v.3.3.1 (R Development Core Team 2017), using package e1071 (Meyer et al. 2014).

The structure of the final SVM model depends on the specific split made between training and test data. For a different training data subset, the optimized values for *cost* and *gamma*, as well as the accompanying support vectors, may change. Such changes may be important, as SVMs are relatively sensitive to even small changes in parameter values. To increase the robustness of the SVM-based projections, we used a process called bagging (Breiman, 1996). The idea of bagging is to generate an ensemble projection, which we generated here by creating 50 different SVM models, using randomized splits between training and test data for each model. As each model yielded

an output map, we could create an ensemble map containing for each pixel the average probability of belonging to the Coralita class. We verified that these average probabilities had converged after 50 iterations (Figure S3).

#### 2.2.4 | Step 4: Threshold determination and accuracy assessment

Converting the continuous probability maps generated in Step 3 into classified maps required setting a threshold probability value above which pixels were assigned to the Coralita class. The optimal threshold value minimizes the frequency of false positives and false negatives and can be found by maximizing the area under the receiver operator characteristic (ROC) curve (e.g., Pouteau et al. 2012). Applying this procedure for each of the 50 maps generated in Step 3 yielded an average optimal threshold probability value of 0.4432, which was then used to create a binary ensemble map. We verified that this optimal threshold probability had converged after 50 iterations (Figure S4). After post-processing (see Supplementary Information), we also calculated four metrics indicating classification accuracy (e.g., Fitzgerald & Lees 1994; Raju et al., 2001): (1) the *producer's accuracy* indicates the likelihood of assigning non-target pixels erroneously to the target class; (2) the *user's accuracy* indicates the likelihood of assigning target pixels erroneously to the not-target class; (3) the *overall prediction success* quantifies the agreement between reference points and the SVM-based classification of the corresponding pixels; (4) the *Kappa statistic* is derived from *overall prediction success*, but also accounts for the probability that pixels were classified (in)correctly by chance. The four metrics were calculated for each map using the test datasets for each of the 50 SVM model iterations. Area under ROC curve and optimal probability thresholds were calculated using the R package ROCR (Sing et al. 2005). Classification accuracy metrics were calculated using the R package caret (Kuhn, 2015).

### 2.3 | Associations between Coralita presence and local environmental variables

To reach the study's second goal, we selected several landscape and environmental variables we hypothesize to be associated with Coralita presence: distance to roads, geomorphological characteristics, and land cover. First, the spread of invasive plants is often associated with disturbance concurrent with human activities and roads present both a conduit for spread and a habitat for establishment and persistence (Arteaga et al. 2009; Christen & Matlack, 2009). Moreover, observations from Coralita's native range suggest that such disturbed areas provide suitable habitat for this species (Burke & DiTommaso, 2011; Muniappan et al. 2002; Vandebroek et al. 2018). Thus, the distance to the nearest road was calculated for each pixel using a digitized roads GIS layer. Second, since Coralita thrives in moist soils (Raju et al., 2001), presence of the species may

be associated with the geomorphology of the landscape, determining where water flows converge and infiltrate (Parolo et al. 2008). To assess geomorphological variables, we computed slope and upslope drainage area, which can be combined to calculate a Topographic Wetness Index (TWI; Beven & Kirkby, 1979). Slope was calculated using a high spatial resolution DTM (Mücher et al., 2014), which was smoothed and resampled to remove noise. From this adjusted DTM we also calculated upslope drainage area and delineated drainage channels in TauDEM v 5.3 (<http://hydrology.usu.edu/taudem/>, Tarboton, 1997). Lastly, the land use and disturbance history

of a site can affect the establishment of invasive plants (Lundgren et al. 2006; Mattingly & Orrock, 2013), with frequently disturbed areas having higher incidence of IAS. On St. Eustatius, there is a long history of land use for agriculture, which has left its legacy in the predominance of disturbed vegetation and land cover types (de Freitas et al. 2014; Hartog, 1976). Based on previous observations of Coralita's affinity to such disturbed areas (Burke & DiTommaso, 2011; Ernst & Ketner, 2007), we hypothesize that Coralita will be found more often in such areas. We assessed the relationship between land cover and Coralita presence with the land cover map

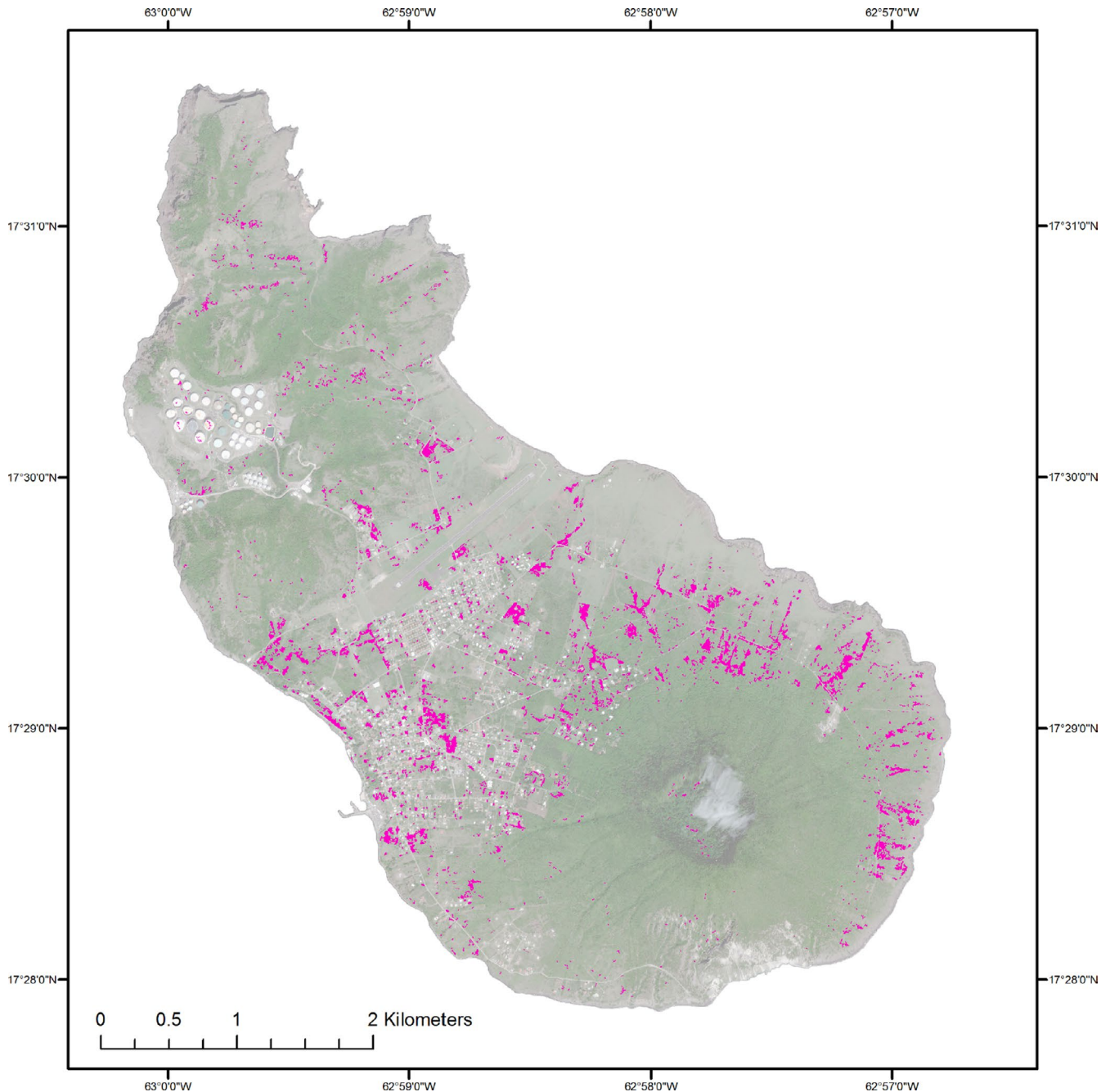


**FIGURE 3** Map of the distribution of Coralita on St. Eustatius. Areas classified as Coralita are shown in pink and are locations where Coralita covers >50% of a pixel (spatial resolution  $2 \times 2$  m). The total area classified as Coralita is 64 ha, or 3.18% of the total land area of St. Eustatius

generated by Helmer et al. (2008), who created a nearly cloud free image of St. Eustatius using a mosaic of Landsat 7 ETM+ images (spatial resolution: 30 m). The image was classified into nine land cover categories on St. Eustatius. In this study, we aggregated these nine land cover categories into five: urban, grasslands, disturbed forest, natural forest, and 'other' land use types (including e.g., cliffs and bare soil).

We tested spatial correlation of Coralita patches with roads, streams, slope, and TWI value as well as the occurrence in the land cover categories. Therefore, we chose one point randomly located in each of the mapped contiguous Coralita patches. As the distribution map contained 1852 Coralita patches, we randomly selected the same number of not-Coralita points for comparison. For each local environmental variable, we compared the distribution of values of Coralita and not-Coralita points using two-sample Kolmogorov–Smirnov tests. We also compared differences in the median score of both groups using Mann–Whitney U tests. For the nominal variable land cover, we compared differences between both groups using a

TABLE 2 Classification accuracy for Coralita SVM model

Index	Mean value	Standard error
Overall prediction success	93.2%	0.56%
Kappa	0.761	0.02
Producer's Accuracy <sub>Coralita</sub>	76.4%	2.01%
Producer's Accuracy <sub>NotCoralita</sub>	97.2%	0.38%
User's Accuracy <sub>Coralita</sub>	86.2%	1.91%
User's Accuracy <sub>NotCoralita</sub>	94.7%	0.50%

Note: Accuracy indices for Coralita SVM classification. Producer's accuracy and user's accuracy for the Coralita class are 76.4% and 86.2%, respectively. Both of these accuracy measurements have a standard error of  $\pm 2\%$ .

Chi-square test. All statistical analyses were performed in MATLAB v 9.0 (MathWorks, 2016).

### 3 | RESULTS

#### 3.1 | Mapping the occurrence patterns of Coralita

Higher scores on the three vegetation indices indicated that Coralita pixels exhibited relatively strong absorption in the Red-edge band (Figure 2; Table 1), as absolute reflectance values in the Red-edge band were relatively high around Coralita pixels (Figure 2; Table 1). Reflectance in the Red band was relatively uniform in the pixels around Coralita (Figure 2; Table 1). Coralita pixels exhibited high reflectance in the  $NIR_1$  band, which were spatially more heterogeneous around Coralita pixels than around not-Coralita pixels (Figure 2; Table 1). A similar spatial pattern was observed for the Blue band (Figure 2; Table 1). These patterns are consistent with observations of Coralita having distinctive bright green leaves (Figure S2), with relatively high chlorophyll content and photosynthetic activity.

According to the resulting classification map produced for August 2014, Coralita was the dominant plant on 64 ha of the island, which translates to 3.18% of the total horizontal land area (Figure 3). The average patch size was  $345 \pm 5 \text{ m}^2$ . The averages and standard errors of classification accuracy metrics are presented in Table 2. The average overall prediction success for this classification was 93.2% (SE  $\pm 0.56\%$ ) while the average Kohen's Kappa statistic was 0.761 (SE  $\pm 0.02$ ). The average producer's accuracy of the Coralita class was 76.4% (SE  $\pm 2.01\%$ ), and the average user's accuracy of the Coralita class was 86.2% (SE  $\pm 1.91\%$ ), whereas the average producer's and user's accuracies of the not-Coralita class were 97.2% (SE  $\pm 0.38\%$ ) and 94.7% (SE  $\pm 0.50\%$ ), respectively.

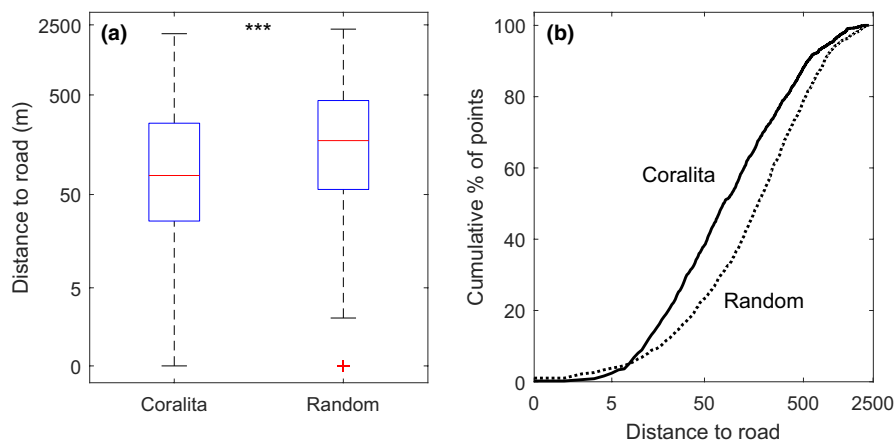


FIGURE 4 Analysis of distance to roads of Coralita patches vs. not-Coralita patches. Patches of the invasive plant Coralita grew closer to the roads of St. Eustatius (Caribbean) than would be expected if the species occurred randomly over the island. (a) Boxplot (with a logarithmic y-axis) showing the median, 25<sup>th</sup> and 75<sup>th</sup> percentiles of distances from the nearest road of  $n = 1852$  points on the island covered by Coralita, compared to  $n = 1852$  randomly selected, non-Coralita points on the island. (b) Cumulative distributions of Coralita points and non-Coralita points. 40% of Coralita locations were within 50 m of a road; 80% of Coralita locations were within 220 m of a road



### 3.2 | Associations between Coralita presence and local environmental variables

Distances to roads were significantly differently distributed for Coralita points and randomly selected not-Coralita points (two-sample Kolmogorov–Smirnov test:  $D_{1852,1852} = 0.197$ ,  $p < 0.001$ ). Coralita occurred closer to roads than expected from a random distribution over the island (Figure 4a; mean distance from roads<sub>Coralita</sub>: 209.8 m (SE  $\pm 7.2$  m), mean distance from roads<sub>Not-Coralita</sub>: 321.0 m (SE  $\pm 9.2$  m), Mann–Whitney U test:  $U_{1852,1852} = 1.3 \times 10^6$ ,  $p < 0.001$ ). Approximately 40% of Coralita locations were within 50 m of a road (for random, non-Coralita points: 116 m, Figure 4b), and approximately 80% of Coralita locations were within 335 m of a road (for random, not-Coralita points: 527 m, Figure 4b; Figure S7).

Slopes, TWI scores, and distances to drainage channels all showed significantly different distributions for Coralita points and randomly selected not-Coralita points (two-sample Kolmogorov–Smirnov tests: Slope:  $D_{1852,1852} = 0.236$ ,  $p < 0.001$ ; TWI:  $D_{1852,1852} = 0.197$ ,  $p < 0.001$ ; Drainage channels:  $D_{1852,1852} = 0.158$ ,  $p < 0.001$ ). Coralita occurred on shallower slopes than expected from a random distribution over the island (Figure 5a; Figure S8; mean slope<sub>Coralita</sub>: 9.9% (SE  $\pm 0.2\%$ ), mean slope<sub>Not-Coralita</sub>: 15.3% (SE  $\pm 0.3\%$ ), Mann–Whitney U test:  $U_{1852,1852} = 1.34 \times 10^6$ ,  $p < 0.001$ ). Coralita also occurred in areas with higher TWI scores (Figure 5b; Figure S9; TWI<sub>Coralita</sub> = 7.3 (SE  $\pm 0.05$ ), TWI<sub>Not-Coralita</sub> = 6.5 (SE  $\pm 0.05$ ), Mann–Whitney U test:  $U_{1852,1852} = 1.27 \times 10^6$ ,  $p < 0.001$ ), and in areas closer to drainage channels (Figure 5c; Figure S10; distance from channels<sub>Coralita</sub>: 87.4 m (SE  $\pm 1.9$  m), distance from channels<sub>Not-Coralita</sub>: 127.7 m (SE  $\pm 2.8$  m), Mann–Whitney U test:  $U_{1852,1852} = 1.37 \times 10^6$ ,  $p < 0.001$ ).

The occurrence of Coralita across land cover types (Figure 6a) was significantly different than expected from a random distribution over the island (Figure 6b,c; Chi-square test:  $\chi_4^2 = 304$ ,  $p < 0.001$ ). Coralita occurred predominantly in specific land cover types: grasslands, disturbed forest, and urban areas. In total, 85% of Coralita's cover appeared in these land cover types, where 60% of cover would be expected for a randomly distributed species (Figure 6b,c). In contrast, the occurrence of Coralita was relatively rare in natural forest. In total, 11% of Coralita's cover appeared within this land cover type, where 29% of cover would be expected for a randomly distributed species (Figure 6).

## 4 | DISCUSSION

We present a cost-effective approach to obtain an accurate and fine-scale distribution of an invasive species over an entire Caribbean island. Knowing the distribution of an invasive species population over an entire land unit is essential for monitoring programs of invasive species (Jones, 2011), while high spatial resolution data is needed to study ecological mechanisms of spread of invasive species patches (Dronova et al. 2017). Although previous studies have demonstrated that SVMs are powerful tools to create accurate classification

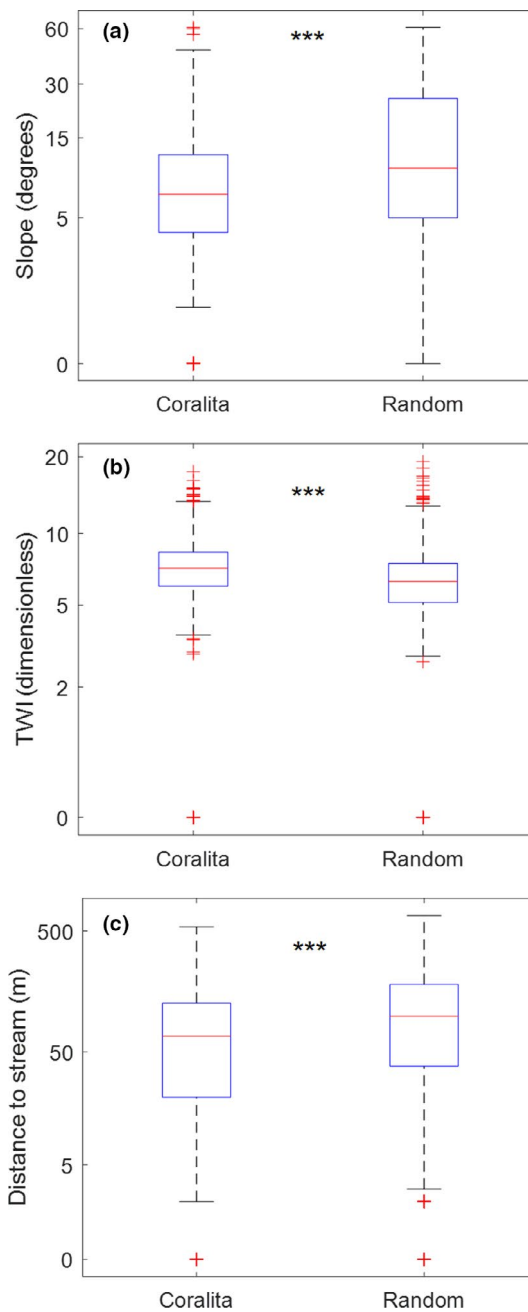


**FIGURE 5** Associations between geomorphological variables and the occurrence of the invasive plant species Coralita on St. Eustatius (Caribbean). Results are shown as boxplots (with logarithmic y-axes) indicating the median, 25<sup>th</sup> and 75<sup>th</sup> percentiles of  $n = 1852$  points on the island covered by Coralita, and  $n = 1852$  randomly selected, not-Coralita points on the island. (a) Patches of the invasive plant Coralita grew in areas with shallower slopes than would be expected if the species occurred randomly over the island. (b) Patches of Coralita grew in moister areas (indicated by Topographic Wetness Index (TWI) scores) than would be expected if the species occurred randomly over the island. (c) Coralita patches occurred closer to drainage channels than would be expected if the species occurred randomly over the island

schemes (Khatami et al. 2016; Mantero et al., 2004; Mountrakis et al. 2011), the potential of these approaches to infer invasive species presence from novel multispectral data sources has remained

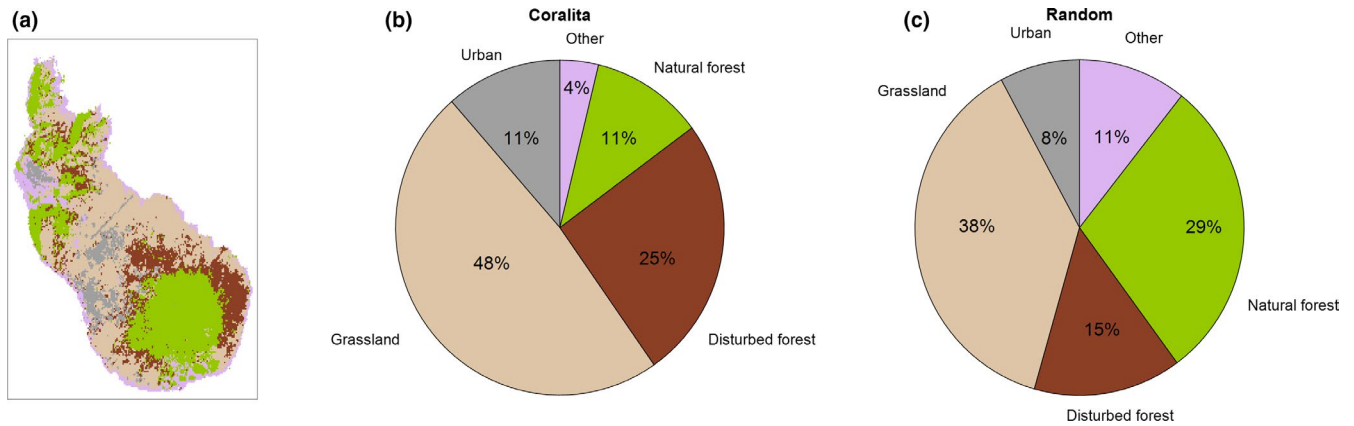


**FIGURE 6** Association between land cover type and the occurrence of the invasive plant species *Coralita* on St. Eustatius (Caribbean). (a) A land cover type map (derived from Helmer et al., 2008) was used to identify the land cover for each of 1852 points occupied by *Coralita*, and for 1852 not-*Coralita* points. (b) Frequency distribution of *Coralita* points across land cover types. (c) Frequency distribution of not-*Coralita* points across land cover types. Comparing of (b) and (c) shows that *Coralita* occurs relatively frequently in grasslands, disturbed forest and urban areas, and relatively rarely in natural forest and other types of land cover (such as coastal, cliffs, sand and rock)

largely unexplored (Royimani et al. 2019). In this study, we reached high accuracy with an SVM classifier of a WorldView-2 image, which could be attributed to the distinct coloring of the target invasive species *Coralita* (Figure 2; Figure S2). Moreover, the prominent inclusion of texture metrics in the classifier suggest that *Coralita* has distinct canopy characteristics that are detectable with multispectral data compared with other land cover types (Figure 2; Figure S2).

We found that *Coralita* is the dominant canopy cover on 64 ha, or 3.18%, of the island. It should be noted, however, that any estimate based on a classification system with <100% accuracy is subject to propagation of error and hence uncertainty (Olofsson et al. 2014). Also, dominant canopy cover is a different metric than appearance, which was reported in previous studies (Berkowitz, 2014; Ernst & Ketner, 2007). Previous estimates of appearance were based on ground-based interpolation of observations made from main and secondary roads (Berkowitz, 2014; Ernst & Ketner, 2007). The spatial grain size used in the latter type of analyses is typically larger than the 2 m by 2 m resolution considered in our study. Comparisons of metrics derived at different spatial grains are subject to Modifiable Area Unit Problem (Jelinski & Wu, 1996; Wong, 2004). Within the context of invasive species analysis, increasing the spatial grain size of observation may lead to increasing estimates of cover based on presence, and decreasing estimates of area dominated. In other words, metrics obtained at different spatial scales provide different kinds of ecological information. In addition, expert-opinion range maps can be prone to errors of commission (Rondinini et al. 2006) because they tend to overestimate occupancy at small spatial scales (Hurlbert & Jetz, 2007; Jetz et al. 2008). On the other hand, despite the relatively high classification accuracy of our map, the unfiltered classification yielded a considerable number of single, isolated pixels classified as being occupied by *Coralita*. Such pixels are typically removed by the application of moving filter approaches (e.g., Hamada et al. 2007), which we also employed in this study (Supplementary Information). Filtering may remove some possibilities for early detection of the invasive species. Moreover, optical data do not penetrate through

the canopy, hindering the detection of subcanopy species except during leaf-off conditions. The presence of *Coralita* under trees and shrubs, even in low densities, may provide important information for managers regarding the recovery potential of vegetation types following disturbance (see e.g. Horvitz et al. 1995, 1998). Although our observations from the field suggest that occurrence of *Coralita* in the understory is rare (E.A. Haber, M.B. Eppinga, and M.J. Wassen, *pers. observations*), the potential impacts may warrant monitoring using alternative, field-based approaches. In terms of methodology, a disadvantage of expert-interpreted maps is the non-transferability of the method (Morrison, 2016), making it difficult to accurately monitor over time. In contrast, an imagery-based classification is both standardized and repeatable, allowing for consistent comparisons of changes in distribution of invasive plants over time. These advantages and constraints of each method should be considered before using distribution maps for management.

Our study enabled a detailed characterization of how the occurrence of *Coralita* on St. Eustatius is associated with local environmental variables, which can be compared to observations from the species' native habitat. In its native habitat in Mexico, *Coralita* is characterized as a roadside weed and its presence is also associated with channels (Burke & DiTommaso, 2011; Vandebroek et al. 2018). We observed similar patterns in the invasive habitat, as *Coralita* grew in relatively close proximity to roads and channels (Figure 4). However, we also observed that *Coralita*'s distribution is not confined to these habitats (Figures 3 and 5). Although it may be difficult for *Coralita* to invade the climax vegetation states that develop under the high precipitation regimes of the northern Caribbean (Figure 6b), the species may benefit from the relatively moist conditions in areas that experienced recent disturbance (van der Burg et al. 2012). Such conditions are ideal habitats for ruderal plant species and species which thrive with disturbance, which include invasive species (Jauni et al. 2015; Lu et al. 2013). Hence, our analyses emphasize recent recommendations for control of *Coralita* in this specific type of Caribbean habitat (Figure 6; Debrot et al., 2018). An important next step to aid

management could focus on creating a habitat suitability model for Coralita on St. Eustatius, which could inform risk assessments of future spread (cf. Jiménez-Valverde et al. 2011). Furthermore, this approach could then be extended to other regions (i.e., Caribbean islands) as well (cf. FitzPatrick et al. 2007).

In the Caribbean biodiversity hotspot, centuries of overharvesting, habitat loss, invasive ungulates, and land conversion for agriculture have drastically reduced the extent of pristine vegetation types such as lowland deciduous forests (Maunder et al. 2008). Although the studied island St. Eustatius is relatively small, its biodiversity is of unique value. It is home to two endemic plant species, the Statia morning glory (*Ipomoea sphenophylla*) and the Statia milkweed (*Gonolobus aloiensis*) (Axelrod, 2017), and the critically endangered Lesser Antillean Iguana (*Iguana delicatissima*). The invasion by Coralita and subsequent habitat alteration may impact organisms at higher trophic levels (Jesse et al. 2020), including negative impacts on the iguana population (Debrot et al. 2014; Powell et al. 2005). More generally, due to Coralita's capacity to overgrow and out-compete other vegetation, including shrubs and trees, it has been characterized as the most problematic invasive plant for several Caribbean islands (van der Burg et al. 2012). The presented approach provides a promising avenue toward monitoring the extent of invasive species distributions, and inferring the ecology of their spread from existing patches, to be tested in future studies.

## ACKNOWLEDGEMENTS

This research was funded by the Dutch Organization for Scientific Research (NWO, grant number 858.14.052) and the Van Eeden Foundation (grant number 201509). We thank the Caribbean Netherlands Science Institute for logistical support. We also thank J. Bekema, B. Bernik, T. de Scisciolo, J. Ellers, W. Jesse, and R. Zilber and the staff of the St. Eustatius National Parks Foundation for fieldwork assistance.

## DATA AVAILABILITY STATEMENT

The data that support the findings of this study are openly available in the Dryad digital repository: <https://doi.org/10.5061/dryad.6wwwpzgmj> (Haber et al. 2021).

## ORCID

Maarten B. Eppinga  <https://orcid.org/0000-0002-1954-6324>

## REFERENCES

- Andrew, M. E., & Ustin, S. L. (2009). Habitat suitability modelling of an invasive plant with advanced remote sensing data. *Diversity and Distributions*, 15, 627–640.
- Arteaga, M. A., Delgado, J. D., Otto, R., Fernández-Palacios, J. M., & Arévalo, J. R. (2009). How do alien plants distribute along roads on oceanic islands? A case study in Tenerife, Canary Islands. *Biological Invasions*, 11, 1071–1086.
- Asner, G., Jones, M. O., Martin, R. E., Knapp, D. E., & Hughes, R. F. (2008). Remote sensing of native and invasive species in Hawaiian forests. *Remote Sensing of Environment*, 112, 1912–1926.
- Asner, G., Knapp, D. E., Otto, R., Kennedy-Bowdoin, T., Jones, M. O., Martin, R. E., Boardman, J., & Hughes, R. F. (2008). Invasive species detection in Hawaiian rainforests using airborne imaging spectroscopy and LiDAR. *Remote Sensing of Environment*, 112, 1942–1955.
- Axelrod, F. S. (2017). *A systematic vademecum to the vascular plants of Sint Eustatius*. BRIT Press.
- Bartuszevige, A. M., & Gorchoy, D. L. (2006). Avian seed dispersal of an invasive shrub. *Biological Invasions*, 8, 1013–1022.
- Bellard, C., Cassey, P., & Blackburn, T. M. (2016). Alien species as a driver of recent extinctions. *Biology Letters*, 12(2), 20150623.
- Berglund, H., Järeemo, J., & Bengtsson, G. (2009). Endemism predicts intrinsic vulnerability to nonindigenous species on Islands. *American Naturalist*, 174, 94–101.
- Berkowitz, B. (2014). *The State of Antigonon leptopus (Corallita) on St. Eustatius in 2014*. STENAPA internal report, St. Eustatius, Caribbean Netherlands.
- Beven, K. J., & Kirkby, M. J. (1979). A physically based, variable contributing area model of basin hydrology. *Hydrological Sciences Bulletin*, 24, 43–69.
- Breiman, L. (1996). Bagging predictors. *Machine Learning*, 24, 123–140.
- Brown, J. H., & Sax, D. F. (2004). An essay on some topics concerning invasive species. *Austral Ecology*, 29, 530–536.
- Burke, J. M., & DiTommaso, A. (2011). Corallita (*Antigonon leptopus*): Intentional introduction of a plant with documented invasive capability. *Invasive Plant Science and Management*, 4, 265–273.
- Cho, M. A., Malahlela, O., & Ramoelo, A. (2015). Assessing the utility WorldView-2 imagery for tree species mapping in South African subtropical humid forest and the conservation implications: Dukuduku forest patch as case study. *International Journal of Applied Earth Observation and Geoinformation*, 38, 349–357.
- Christen, D. C., & Matlack, G. R. (2009). The habitat and conduit functions of roads in the spread of three invasive plant species. *Biological Invasions*, 11, 453–465.
- Cortes, C., & Vapnik, V. (1995). Support-Vector Networks Editor. *Machine Learning*, 20, 273–297.
- D'Antonio, C. M., & Dudley, T. L. (2011). Biological invasions as agents of change on Islands versus Mainlands. In P. M. Vitousek, L. L. Loope, & H. Adersen (Eds.), *Islands: Biological diversity and ecosystem function* (pp. 103–121). Springer-Verlag Berlin.
- de Freitas, J. A., Rojer, A. C., Nijhof, B. S. J., & Debrot, A. O. (2014). *A landscape ecological vegetation map of Sint Eustatius (Lesser Antilles)*. Royal Netherlands Academy of Arts and Sciences.
- Debrot, A. O., Boman, E. B., Piontek, S., & Madden, H. (2014). Iguana delicatissima (Lesser Antillean Iguana) reproduction. *Herpetological Review*, 45, 129–130.
- Debrot, A. O., Hekens, R. J. H. G., & Verweij, P. J. F. M. (2018). *Staat van instandhouding van de natuur van Caribisch Nederland*. Wageningen Marine Research Report C086/17, Wageningen, The Netherlands.
- Dronova, I., Spotswood, E. N., & Suding, K. N. (2017). Opportunities and constraints in characterizing landscape distribution of an invasive grass from very high resolution multi-spectral imagery. *Frontiers in Plant Science*, 8, 1–17.
- Eppinga, M. B., & Pucko, C. A. (2018). The impact of hurricanes Irma and Maria on the forest ecosystems of Saba and St. Eustatius, northern Caribbean. *Biotropica*, 50, 723–728.
- Ernst, J. J., & Ketner, P. (2007). *Study on the ecology and possible control methods of the invasive plant species Antigonon leptopus (Corallita or Mexican Creeper)*. ABC Research Report.
- Fitzgerald, R. W., & Lees, B. G. (1994). Assessing the classification accuracy of multisource remote sensing data. *Remote Sensing of Environment*, 47, 362–368.
- FitzPatrick, M. C., Weltzin, J. F., Sanders, N. J., & Dunn, R. R. (2007). The biogeography of prediction error: Why does the introduced range of the fire ant overpredict its native range? *Global Ecology and Biogeography*, 16, 24–33.
- Gottschalk, T. K., Aue, B., Hotes, S., & Ekschmitt, K. (2011). Influence of grain size on species-habitat models. *Ecological Modelling*, 222, 3403–3412.

- Haber, E. A., Santos, M. J., Leitão, P. J., Schwieder, M., Ketner, P., Ernst, J., Rietkerk, M., Wassen, M. J., & Eppinga, M. B. (2021). Data from: High spatial resolution mapping identifies habitat characteristics of the invasive vine *Antigonon leptopus* on St. Eustatius (Lesser Antilles). Dryad Digital Repository. <http://doi.org/10.5061/dryad.6wwpzgmxj>
- Hamada, Y., Stow, D. A., Coulter, L. L., Jafolla, J. C., & Hendricks, L. W. (2007). Detecting Tamarisk species (*Tamarix* spp.) in riparian habitats of Southern California using high spatial resolution hyperspectral imagery. *Remote Sensing of Environment*, *109*, 237–248.
- Haralick, R. M., Shanmugam, K., & Dinstein, I. (1973). Textural features for image classification. *IEEE Transactions on Systems, Man, and Cybernetics*, *3*, 610–621.
- Hartog, J. (1976). *History of St. Eustatius*. Central USA Bicentennial Committee of the Netherlands Antilles, distributors: De Wit Stores N.V.
- He, K. S., Rocchini, D., Neteler, M., & Nagendra, H. (2011). Benefits of hyperspectral remote sensing for tracking plant invasions. *Diversity and Distributions*, *17*, 381–392.
- Helmer, E. H., Kennaway, T. A., Pedreros, D. H., Clark, M. L., Marciano-Vega, H., Tieszen, L. L., Przyucki, T. R., Schill, S. R., & Carrington, C. M. S. (2008). Land cover and forest formation distributions for St. Kitts, Nevis, St. Eustatius, Grenada and Barbados from decision tree classification of cloud-cleared satellite imagery. *Caribbean Journal of Science*, *44*, 175–198.
- Horler, D. N. H., Dockray, M., Barber, J., & Barringer, A. R. (1983). Red edge measurements for remotely sensing plant chlorophyll content. *Advances in Space Research*, *3*, 273–277.
- Horvitz, C. C., McMann, S., & Freedman, A. (1995). Exotics and hurricane damage in three hardwood hammocks in Dade County Parks, Florida. *Journal of Coastal Research*, *21*, 145–158.
- Horvitz, C. C., Pascarella, J. B., McMann, S., Freedman, A., & Hofstetter, R. H. (1998). Functional roles of invasive non-indigenous plants in hurricane-affected subtropical. *Ecological Applications*, *8*, 947–974.
- Huang, C., & Asner, G. P. (2009). Applications of remote sensing to alien invasive plant studies. *Sensors*, *9*, 4869–4889.
- Hurlbert, A. H., & Jetz, W. (2007). Species richness, hotspots, and the scale dependence of range maps in ecology and conservation. *Proceedings of the National Academy of Sciences of the United States of America*, *104*, 13384–13389.
- Jauni, M., Gripenberg, S., & Ramula, S. (2015). Non-native plant species benefit from disturbance: A meta-analysis. *Oikos*, *124*, 122–129.
- Jelinski, D. E., & Wu, J. (1996). The modifiable areal unit problem and implications for landscape ecology. *Landscape Ecology*, *11*, 129–140.
- Jesse, W. A., Molleman, J., Franken, O., Lammers, M., Berg, M. P., Behm, J. E., Helmus, M. R., & Ellers, J. (2020). Disentangling the effects of plant species invasion and urban development on arthropod community composition. *Global Change Biology*, *26*(6), 3294–3306.
- Jetz, W., Sekercioglu, C. H., & Watson, J. E. M. (2008). Ecological correlates and conservation implications of overestimating species geographic ranges. *Conservation Biology*, *22*, 110–119.
- Jiménez-Valverde, A., Peterson, A. T., Soberón, J., Overton, J., Aragón, P., & Lobo, J. M. (2011). Use of niche models in invasive species risk assessments. *Biological Invasions*, *13*, 2785–2797.
- Jones, J. P. G. (2011). Monitoring species abundance and distribution at the landscape scale. *Journal of Applied Ecology*, *48*, 9–13.
- Khatami, R., Mountrakis, G., & Stehman, S. V. (2016). A meta-analysis of remote sensing research on supervised pixel-based land-cover image classification processes: General guidelines for practitioners and future research. *Remote Sensing of Environment*, *177*, 89–100.
- Kuhn, M. (2015). Package “caret”: Classification and regression training. *Astrophysics Source Code Library*, *1*, 05003.
- Lu, M., Huang, J., Chung, Y., & Huang, C. (2013). Modeling the invasion of a Central American Mimosoid tree species (*Leucaena leucocephala*) in a tropical coastal region of Taiwan. *Remote Sensing Letters*, *4*, 485–493.
- Lundgren, M. R., Small, C. J., & Dreyer, G. D. (2006). Influence of land use and site characteristics on invasive plant abundance in the Quinebaug Highlands of Southern New England. *Northeastern Naturalist*, *11*, 313–332.
- Mantero, P., Moser, G., & Serpico, S. B. (2004). *Partially supervised classification of remote sensing images using SVM-based probability density estimation*. In 2003 IEEE Workshop on Advances in Techniques for Analysis of Remotely Sensed Data. pp. 327–336.
- MathWorks. (2016). MATLAB 9.0. The MathWorks Inc., Natick, Massachusetts, United States.
- Mattingly, W. B., & Orrock, J. L. (2013). Historic land use influences contemporary establishment of invasive plant species. *Oecologia*, *172*, 1147–1157.
- Maunder, M., Leiva, A., Santiago-Valentín, E., Stevenson, D. W., Acevedo-Rodríguez, P., Meerow, A. W., Mejía, M., Clubbe, C., & Francisco-Ortega, J. (2008). Plant conservation in the Caribbean Island biodiversity hotspot. *Botanical Review*, *74*, 197–207.
- McKinney, M. L., & Lockwood, J. L. (1999). Biotic homogenization: A few winners replacing many losers in the next mass extinction. *Trends in Ecology & Evolution*, *14*, 450–453.
- Meyer, D., Dimitriadou, E., Hornik, K., Weingessel, A., Chang, C.-C., & Lin, C.-C. (2014). Package “e1071”: Misc functions of the department of statistics, probability theory group. Vienna, Austria: TU Wien.
- Morrison, L. W. (2016). Observer error in vegetation surveys: A review. *Journal of Plant Ecology*, *9*, 367–379.
- Mountrakis, G., Im, J., & Ogole, C. (2011). Support vector machines in remote sensing: A review. *ISPRS Journal of Photogrammetry and Remote Sensing*, *66*, 247–259.
- Mücher, S., Jonker, D., Stuijver, J., Kramer, H., & Meesters, E. (2014). *Production of digital terrain models for the Dutch Caribbean*. Alterra Report 2569, Wageningen, The Netherlands.
- Muniappan, R., Cruz, J., & Bamba, J. (2002). Invasive plants and their control in Micronesia. *Micronesica Supplement*, *6*, 85–92.
- Myers, N., Mittermeier, R. A., Mittermeier, C. G., Da Fonseca, G. A. B., & Kent, J. (2000). Biodiversity hotspots for conservation priorities. *Nature*, *403*, 845–850.
- Nouri, H., Beecham, S., Anderson, S., & Nagler, P. (2014). High spatial resolution WorldView-2 imagery for mapping NDVI and its relationship to temporal urban landscape evapotranspiration factors. *Remote Sensing*, *6*, 580–602.
- Olden, J. D., Poff, N. L. R., Douglas, M. R., Douglas, M. E., & Fausch, K. D. (2004). Ecological and evolutionary consequences of biotic homogenization. *Trends in Ecology & Evolution*, *19*, 18–24.
- Olofsson, P., Foody, G. M., Herold, M., Stehman, S. V., Woodcock, C. E., & Wulder, M. A. (2014). Good practices for estimating area and assessing accuracy of land change. *Remote Sensing of Environment*, *148*, 42–57.
- Oumar, Z., & Mutanga, O. (2013). Using WorldView-2 bands and indices to predict bronze bug (*Thaumastocoris peregrinus*) damage in plantation forests. *International Journal of Remote Sensing*, *34*, 2236–2249.
- Parolo, G., Rossi, G., & Ferrarini, A. (2008). Toward improved species niche modelling: *Arnica montana* in the Alps as a case study. *Journal of Applied Ecology*, *45*, 1410–1418.
- Pouteau, R., Meyer, J. Y., Taputuarai, R., & Stoll, B. (2012). Support vector machines to map rare and endangered native plants in Pacific islands forests. *Ecological Informatics*, *9*, 37–46.
- Powell, R., Henderson, R. W., & Parmerlee, J. S. S. (2005). *The reptiles and amphibians of the Dutch Caribbean: St. Eustatius, Saba, and St. Maarten*. Reptile Education and Research Publishing.
- Raju, A. J. S., Raju, V. K., Victor, P., & Naidu, S. A. (2001). Floral ecology, breeding system and pollination in *Antigonon leptopus* L. (Polygonaceae). *Plant Species Biology*, *16*(2), 159–164.
- R Development Core Team. (2017). R: A language and environment for statistical computing. R Foundation for Statistical Computing.
- Robinson, T. P., Wardell-Johnson, G. W., Pracilio, G., Brown, C., Corner, R., & van Klinken, R. D. (2016). Testing the discrimination and



- detection limits of WorldView-2 imagery on a challenging invasive plant target. *International Journal of Applied Earth Observation and Geoinformation*, 44, 23–30.
- Rojer, A. (1997). *Biological inventory of Sint Eustatius*. Carmabi Foundation.
- Rondinini, C., Wilson, K. A., Boitani, L., Grantham, H., & Possingham, H. P. (2006). Tradeoffs of different types of species occurrence data for use in systematic conservation planning. *Ecology Letters*, 9, 1136–1145.
- Royimani, L., Mutanga, O., Odindi, J., Dube, T., & Matongera, T. N. (2019). Advancements in satellite remote sensing for mapping and monitoring of alien invasive plant species (AIPs). *Physics and Chemistry of the Earth*, 112, 237–245.
- Rumpf, T., Mahlein, A.-K., Steiner, U., Oerke, E.-C., Dehne, H.-W., & Plümer, L. (2010). Early detection and classification of plant diseases with Support Vector Machines based on hyperspectral reflectance. *Computers and Electronics in Agriculture*, 74, 91–99.
- Sakai, A. K., Allendorf, F. W., Holt, J. S., Lodge, D. M., Molofsky, J., With, K. A., Baughman, S., Cabin, R. J., Cohen, J. E., Ellstrand, N. C., McCauley, D. E., O'Neil, P., Parker, I. M., Thompson, J. N., & Weller, S. G. (2001). The population biology of invasive species. *Annual Review of Ecology and Systematics*, 32, 305–332.
- Santos, M. J., Khanna, S., Hestir, E. L., Greenberg, J. A., & Ustin, S. L. (2016). Measuring landscape-scale spread and persistence of an invaded submerged plant community from airborne Remote sensing. *Ecological Applications*, 26, 1733–1744.
- Santos, M. J., Anderson, L. W., & Ustin, S. L. (2011). Effects of invasive species on plant communities: an example using submersed aquatic plants at the regional scale. *Biological Invasions*, 13, 443–457.
- Santos, M. J., & Ustin, S. L. (2018). *Spectral identification of native and non-native plant species for biodiversity assessments*. In IGARSS 2018 - 2018 IEEE International Geoscience and Remote Sensing Symposium. pp. 3420–3423, IEEE.
- Sax, D. F., Gaines, S. D., & Brown, J. H. (2002). Species invasions exceed extinctions on islands worldwide: A comparative study of plants and birds. *American Naturalist*, 160, 766–783.
- Schwieder, M., Leitão, P. J., Suess, S., Senf, C., & Hostert, P. (2014). Estimating fractional shrub cover using simulated enmap data: A comparison of three machine learning regression techniques. *Remote Sensing*, 6, 3427–3445.
- Sha, Z., & Bai, Y. (2013). *Mapping grassland vegetation cover based on support vector machine and association rules*. Ninth International Conference on Natural Computation (ICNC), pp. 44–49.
- Sing, T., Sander, O., Beerwinkel, N., & Lengauer, T. (2005). ROC: Visualizing classifier performance in R. *Bioinformatics*, 21, 3940–3941.
- Sloan, S., Jenkins, C. N., Joppa, L. N., Gaveau, D. L. A., & Laurance, W. F. (2014). Remaining natural vegetation in the global biodiversity hotspots. *Biological Conservation*, 177, 12–24.
- Sluiter, R., & Pebesma, E. J. (2010). Comparing techniques for vegetation classification using multi- and hyperspectral images and ancillary environmental data. *International Journal of Remote Sensing*, 31, 6143–6161.
- Smith, S. R., Múcher, C. A., Debrot, A. O., Roupioz, L., Meesters, H. W. G., Hazeu, G. W., & Davaasuren, N. (2013). *Use of satellite data for the monitoring of species on Saba and St. Eustatius*. IMARES, Wageningen UR.
- Somers, B., & Asner, G. P. (2012). Invasive species mapping in Hawaiian rainforests using multi-temporal Hyperion spaceborne imaging spectroscopy. *IEEE Journal of Selected Topics in Applied Earth Observations and Remote Sensing*, 6, 351–359.
- Somers, B., & Asner, G. P. (2013). Multi-temporal hyperspectral mixture analysis and feature selection for invasive species mapping in rainforests. *Remote Sensing of Environment*, 136, 14–27.
- Stoffers, A. L. (1956). *The vegetation of the Netherlands Antilles*. Utrecht, The Netherlands: Botanisch museum en herbarium Utrecht.
- Tarantino, C., Casella, F., Adamo, M., Lucas, R., Beierkuhnlein, C., & Blonda, P. (2019). *Ailanthus altissima* mapping from multi-temporal very high resolution satellite images. *ISPRS Journal of Photogrammetry and Remote Sensing*, 147, 90–103.
- Tarboton, D. G. (1997). A new method for the determination of flow directions and upslope areas in grid elevation models. *Water Resources Research*, 33, 309–319.
- Turbelin, A. J., Malamud, B. D., & Francis, R. A. (2017). Mapping the global state of invasive alien species: Patterns of invasion and policy responses. *Global Ecology and Biogeography*, 26, 78–92.
- Ustün, B., Melsens, W. J., & Buydens, L. M. C. (2007). Visualisation and interpretation of Support Vector Regression models. *Analytica Chimica Acta*, 595, 299–309.
- van Andel, T., van der Hoorn, B., Stech, M., Arostegui, S. B., & Miller, J. (2016). A quantitative assessment of the vegetation types on the island of St. Eustatius, Dutch Caribbean. *Global Ecology and Conservation*, 7, 59–69.
- van der Burg, W. J., de Freitas, J. A., Debrot, A. O., & Lotz, L. A. P. (2012). *Naturalised and invasive alien plant species in the Caribbean Netherlands: status, distribution, threats, priorities and recommendations*. Plant Research International.
- Vandebroek, I., Picking, D., Lewis, P. A., Oberli, A., Aiken, S., Mitchell, S., & Boom, B. (2018). A review of Coralilla (*Antigonon leptopus*): An invasive and popular urban bush medicine in Jamaica. *Economic Botany*, 72, 229–245.
- Veenenbos, J. S. (1955). *A soil and land capability survey of St. Maarten, St. Eustatius, and Saba*. Publ. Found. Sci. Res. Sur. Neth. Ant., Utrecht, The Netherlands.
- Vilà, M., Espinar, J. L., Hejda, M., Hulme, P. E., Jarošík, V., Maron, J. L., Pergl, J., Schaffner, U., Sun, Y., & Pyšek, P. (2011). Ecological impacts of invasive alien plants: A meta-analysis of their effects on species, communities and ecosystems. *Ecology Letters*, 14, 702–708.
- Walter-Shea, E. A., & Norman, J. M. (1991). Leaf optical properties. In R. B. Myneni & J. Ross (Eds.), *Photon-vegetation interactions* (pp. 229–251). Springer-Verlag.
- Wolf, A. (2010). *Using WorldView 2 Vis-NIR MSI imagery to support land mapping and feature extraction using normalized difference index ratios*. DigitalGlobe 8-Band Research Challenge, pp. 1–13.
- Wong, D. W. S. (2004). The modifiable areal unit problem (MAUP). In A. Fotheringham & P. A. Rogerson (Eds.), *The SAGE handbook of spatial analysis* (5th ed., pp. 105–123). SAGE Publications Ltd.
- Xun, L., & Wang, L. (2015). An object-based SVM method incorporating optimal segmentation scale estimation using Bhattacharyya Distance for mapping salt cedar (*Tamarisk* spp.) with QuickBird imagery. *GisScience & Remote Sensing*, 52, 257–273.

## SUPPORTING INFORMATION

Additional supporting information may be found online in the Supporting Information section.

**How to cite this article:** Haber EA, Santos MJ, Leitão PJ, et al.

High spatial resolution mapping identifies habitat characteristics of the invasive vine *Antigonon leptopus* on St. Eustatius (Lesser Antilles). *Biotropica*. 2021;53:941–953.

<https://doi.org/10.1111/btp.12939>